High-performance graphene-based carbon nanofiller/polymer composites for piezoresistive sensor applications

Costa, P.; Nunes-Pereira, J.; Oliveira, J; Agostinho Moreira, J.; Carabineiro, S.A.C.; Buijnsters, J.G.; Lanceros-Mendez, S

DOI
10.1016/j.compscitech.2017.11.001

Publication date
2017

Document Version
Final published version

Published in
Composites Science and Technology

Citation (APA)
Costa, P., Nunes-Pereira, J., Oliveira, J., Agostinho Moreira, J., Carabineiro, S. A. C., Buijnsters, J. G., & Lanceros-Mendez, S. (2017). High-performance graphene-based carbon nanofiller/polymer composites for piezoresistive sensor applications. *Composites Science and Technology*, *153*, 241-252. https://doi.org/10.1016/j.compscitech.2017.11.001

Composites Science and Technology 153 (2017) 241–252

Contents lists available at ScienceDirect

Composites Science and Technology

journal homepage: http://www.elsevier.com/locate/compscitech

High-performance graphene-based carbon nanofiller/polymer composites for piezoresistive sensor applications

P. Costa [a, b, *], J. Nunes-Pereira [a, c], J. Oliveira [a, d], J. Silva [e], J. Agostinho Moreira [f], S.A.C. Carabineiro [g], J.G. Buijnsters [h], S. Lanceros-Mendez [i, j]

[a] Centre of Physics, University of Minho, 4710-057 Braga, Portugal
[b] Institute for Polymers and Composites IPC/I3N, University of Minho, 4800-058 Guimarães, Portugal
[c] C-MAST – Centre for Mechanical and Aerospace Science and Technologies, Universidade da Beira Interior, 6200-001 Covilhã, Portugal
[d] Algoritmi Research Center, University of Minho, Campus de Azurém, 4800-058 Guimarães, Portugal
[e] CFisUC, Department of Physics, University of Coimbra, Rua Larga, Coimbra, Portugal
[f] IFIMUP and IN-Institute of Nanotechnology, Department of Physics and Astronomy, Faculty of Sciences, University of Porto, Rua do Campo Alegre, 678, Porto, Portugal
[g] Laboratório de Catálise e Materiais (LCM), Laboratório Associado LSRE-LCM, Faculty of Engineering, University of Porto, Rua Dr. Roberto Frias s/n, 4200-465 Porto, Portugal
[h] Department of Precision and Microsystems Engineering, Research Group of Micro and Nano Engineering, Delft University of Technology, Mekelweg 2, 2628 CD Delft, The Netherlands
[i] BCMaterials, Parque Científico y Tecnológico de Bizkaia, 48160 Derio, Spain
[j] IKERBASQUE, Basque Foundation for Science, 48013 Bilbao, Spain

ARTICLE INFO

Article history:
Received 5 September 2017
Received in revised form
25 October 2017
Accepted 1 November 2017
Available online 5 November 2017

Keywords:
Functional composites
Polymer-matrix composites (PMCs)
Electrical properties
Scanning electron microscopy (SEM)
Casting

ABSTRACT

Poly(vinylidene fluoride) (PVDF) composites with different carbonaceous nanofillers, prepared by solution casting, were studied their chemical, mechanical, electrical and electro-mechanical properties evaluated. Few-layer graphene (FLG) nanoplatelets (G-NPL), graphene oxide (GO) and reduced graphene oxide (rGO) and single-walled carbon nanohorns (SWCNH)) were found to have a strong influence in the overall properties of the composites prepared with up to 5 wt% nanofiller contents. The mechanical strain of carbonaceous nanofillers/PVDF composites decreases from 15% to near 5% of maximum strain. The electrical percolation threshold depends on the nanofiller type, being below 1 wt% for rGO and near 2 wt% for the remaining nanofillers. The electrical conductivity shows a maximum increase of nine orders of magnitude, from $\sigma \approx 5 \times 10^{-11}$ S/m of pure PVDF to $\sigma \approx 1 \times 10^{-2}$ S/m for rGO/PVDF composites with 5 wt% nanofillers. The conduction mechanism being related to hopping between the carbonaceous nanofillers for concentrations higher than the percolation threshold.

Furthermore, the composites show electro-mechanical properties, except for G-NPL materials, with rGO/PVDF composites with 5 wt% nanofiller content showing higher Gauge factor (GF) values, reaching GF≈ 11 for deformations between 0.5 and 2 mm in 4-point bending experiments. These results demonstrate the suitability of the composites for strain sensing applications.

1. Introduction

The study of polymer composites containing conductive or insulating materials is an area of increasing interest [1]. In particular, carbon nanofiller/polymer nanocomposites have been intensively studied due to their application potential, as they allow to tailor the mechanical and electrical properties of the composite by varying carbon nanofiller concentration, aspect ratio and dispersion [2].

Models have been developed that can predict, to some extent, the effect of adding conductive fillers to a dielectric matrix on the electrical and dielectric properties [3]. The effective mean-field medium concept is the foundation for most of the empirical models. The main drawback of these models is that they fail to predict the composite electric behavior near the percolation threshold, defined as the critical point where the physical

* Corresponding author.University of Minho,Centre of Physics, Campus de Gualtar, 4710-057 Braga, Portugal.
E-mail address: pcosta@fisica.uminho.pt (P. Costa).

https://doi.org/10.1016/j.compscitech.2017.11.001
0266-3538/

properties show singularities and scaling behavior [4,5].

In the past years, a new set of emerging nanomaterials, such as nanocarbonaceous, nanodiamonds and functional nanocomposites with novel structure-dependent functional properties have been developed, being interesting both for fundamental research and advanced applications [6,7]. Among the most interesting functional properties of those materials the electro-mechanical ones stands out, as they allow the development of sensors and actuators, with applications in consumer electronics and portable devices, among others [6].

In this context, piezoresistive nanofillers/polymer composites are being strongly investigated due to their exceptional mechanical, electrical and electro-mechanical properties. Particularly, the focus has been on the intrinsic properties of the carbonaceous nanofillers, such as electrical properties and high aspect ratio [8,9]. The most studied carbon nanostructures have been carbon nanofibers (CNF) [10], carbon nanotubes (CNT) [11] and, in recent years, graphene [11,12]. More recently, novel carbonaceous nanomaterials such as single-walled carbon nanohorns (SWCNH) have been reported with distict geometries [10,13], intrinsic mechanical (tensile strength) and electrical properties (electrical conductivity), being quite different from the remaining few-layer graphene materials with different chemical treatments [10] as reduction or oxidation.

Typically, the carbonaceous nanofillers are used for improving mechanical properties and electrical or ionic conductivity of polymer matrices with low electrical percolation thresholds [8,14], the electro-mechanical sensitivity is becoming particularly targeted for study due to their superior response when compared to the strain gages commercial sensors [8,15]. The overall properties of carbon nanoallotropes/polymer composites strongly depend on polymer type and processing method, nanofiller type, degree of aggregation and orientation [16]. This dependence is particularly relevant for the percolation threshold concentration, being the parameter most critical in determining electrical properties and, therefore, the functionality of the composites [17,18].

The percolation threshold concentration is particularly relevant for the development of composites, as they typically show the largest electro-mechanical response-variation of the electrical resistivity when a strainis applied to the material, at concentrations around the percolation threshold [19]. In the case of carbon nanofiller/polymer composites, this effect is mainly attributed (in addition of the geometrical effect) to variations of the conductive network with strain due to loss of contact between the fillers, tunneling or hopping effects in neighboring fillers and/or conductivity variations due to the strain of the different carbonaceous, for example [17,20].

Several strategies and materials have been used for the development of electro-mechanical polymer composites as sensors to detect several external stimulus, including strain, pressure, temperature or light [21]. The electrical resistance variation with external stimulus enables a large range of applications to the piezoresistive composites as strain/pressure sensors in artificial intelligence, electronic devices and industrial production [22]. Typical metal strain gages and silicon piezoresistive sensors present interesting properties but their mechanical properties limit their use [15]. Stretchable or high flexible piezoresistive sensors are fabricated using polymers as matrix and conductive fillers as reinforcement materials [23]. Conductive carbonaceous nanofillers such as graphite, carbon black (CB), graphene, CNF and CNT have been widely employed [18,24], or combination thereof CNT are the most widely used due to their intrinsic electrical properties and geometry, as high aspect ratio, with higher piezoresistive sensitivity [22], although the difficulty to disperse and the high production cost limit their widespread use [22]. In order to increase the overall properties of the composites, better dispersion of carbon nanofillers in the polymer matrix is essential.

Several preparation methods have been developed to manufacture of nanofillers/polymer composites, such as in-situ polymerization, extrusion, solution blending, and electrospinning [24,25]. Solution blending is an excellent method to prepare inks to print by inkjet, screen and spray print, or other methods as roll-to-roll [15,26]. These methods allow printing these materials at a large scale [15,26]. The sensitivity of electro-mechanical properties of carbon nanofillers/PVDF composites depends on the processing method, type of carbon nanofillers and content in composites and may range between 1 to near 200 [27,28].

For the production of flexible or stretchable sensors, elastomers and thermoplastic polymers are the most widely used as matrices [2]. Within the thermoplastics, poly(vinylidene fluoride) (PVDF) and its copolymers have suitable electroactive properties to produce sensors and actuators. PVDF is a semicrystalline polymer with five possible crystalline phases, the most technologically relevant and investigated being the non-polar α-PVDF and the polar β-PVDF, which are the most electrically active phases. Furthermore, PVDF presents good mechanical and chemical properties, weather resistance, and excellent properties associated to their polar crystalline forms [29].

In this sense, the incorporation of novel carbonaceous nanofillers, such as single wall carbon nanohorns, FLG nanoplatelets and treated graphene (oxided and reduced), into PVDF matrices in order to tune and optimize the electro-mechanical behavior and response of the composites is a major challenge that constitutes the focus of this work. The overall properties of the composites will be assessed in view of their applicability as electro-mechanical sensors for bending strain detecting. These materials represent a promising alternative to strain gauge sensors due to their higher GF and simple processing and integration into devices.

2. Materials and methods

2.1. Materials

Commercial Solef 1010 poly(vinylidene fluoride) (PVDF) with Mw = 352,000 g/mol was supplied by Solvay, Inc. (Belgium). The graphene-based nanofillers used are illustrated in Fig. 1. Single walled carbon nanohorns (SWCNH) were supplied by Carbonium (Italy) and consist in tiny graphene sheets, wrapped to form horn-shaped cones with a half fullerene cap, having 30–50 nm length and 3–5 nm diameter. Few-layer graphene oxide, reduced graphene oxide and nanoplatelets were obtained from The Graphene Box (Spain). Graphene oxide (GO) had 99% of purity and a

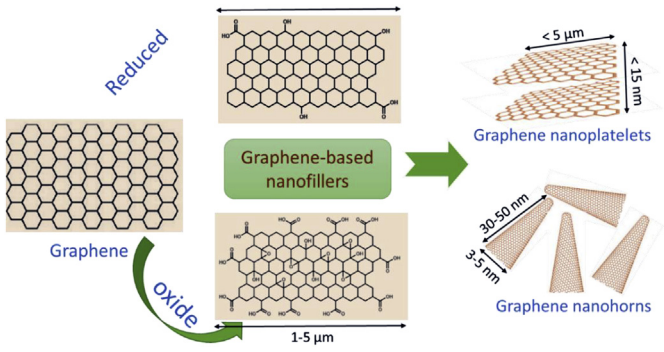

Fig. 1. Illustration of the graphene-based nanofillers with different structures, chemical treatments, geometries and dimensions used for the preparation of the composites. The dimensions of the FLG oxide (GO), reduced graphene oxide (rGO), graphene nanoplatelets (G-NPL) and single-walled carbon nanohorns (SWCNH) are indicated.

volumetric mass density of 0.26 g/cm^3, with 1–5 μm of diameter and a thickness between 0.8 and 1.2 nm. Reduced few-layer graphene oxide (rGO) had >99% of purity with 1–2 layers and 1–5 μm of dimension. rGO were obtained by thermal shock reduction. The few-layer graphene nanoplatelets (G-NPL) showed less than 15 nm of thickness and 5 μm of diameter.

These materials were used to develop polymer composites up to 5 wt% (weight percentage) of carbonaceous nanofillers in the PVDF polymer matrix. The solvent N,N-dimethylformamide (DMF, 99.5%) was purchased from Merck.

2.2. Composite preparation

Before preparation of the composites materials, the nanofillers and polymer were dried at 60 °C in an oven and kept on a desiccator. Polymer films with thicknesses between 40 and 65 μm were produced by solvent casting method mixing different amounts of the carbonaceous nanofillers (0; 0.25; 0.5; 1; 2; 5 wt%) with 9.5 ml of DMF. The solutions were placed in an ultrasound bath (ATU, Model ATM40-3LCD) for 4 h in order to optimize nanofillers deagglomeration and dispersion. After this step, 1g of PVDF (10/90 v/v polymer/solvent ratio) was added to the nanofillers/solvent solution and placed in a magnetic stirrer for complete dissolution of the polymer (about 2 h at 30 °C).

Flexible films were obtained by doctor blade technique by spreading the solution on a clean glass substrate. Complete solvent evaporation and polymer crystallization was performed by melting the samples at 210 °C for 15 min and cooling down to room temperature in a conventional oven (ED 23 Binder). This procedure produces PVDF films in the α-phase.

2.3. Sample characterization

Scanning electron microscopy (SEM) surface and cross section images were obtained with a NanoSEM - FEI Nova 200 (FEG/SEM) equipment with an accelerating voltage of 10 kV, which was used to evaluate the dispersion of the nanofillers within the polymer matrix. The samples in cross section were cut after immersion in liquid nitrogen at temperatures below the glass transition. Then, the samples were coated with a thin gold layer using a sputter coating (Polaron, model SC502 sputter coater).

Fourier transformed infrared spectroscopy (FTIR) analysis was performed with a Jasco FT/IR-4100 in the attenuated total reflectance mode (ATR), at room temperature. FTIR spectra were collected from 4000 to 600 cm^{-1} after 64 scans with a resolution of 4 cm^{-1}.

Raman spectra were recorded at room temperature by using an Olympus microscope and a 50× objective. Excitation was carried out using the 514.5 nm polarized line of an Ar^+ laser, with an incident power of about 16 mW impinging on the sample. The acquisition time for each measurement was set at 120 s and with two/three scans. The scattered light was analyzed using a T64000 Jobin-Yvon spectrometer operating in a triple subtractive mode and equipped with a liquid nitrogen cooled CCD detector, in a Stokes frequency range from 200 to 2000 cm^{-1} [30]. In order to obtain information regarding the homogeneity of our samples, the Raman spectra were recorded at several different positions on the sample surfaces. No significant differences were detected and the results presented in the following are representative of the whole samples.

Textural characterization of the samples was performed by N_2 adsorption-desorption at -196 °C with a Quantachrome NOVA 4200e apparatus. The Brunauer–Emmett–Teller (BET) equation was applied to determine the apparent surface area [31].

X-ray photoelectron spectroscopy (XPS) analyses were performed on a VG Scientific ESCALAB 200A spectrometer using Al Kα radiation (1486.6 eV). The charge effect was corrected taking the C 1s peak as a reference (binding energy of 285 eV). CASAXPS software was used for data analysis.

Mechanical measurements were performed on a universal testing machine (Shimadzu model AG-IS) at room temperature with a load cell of 500 N, in tensile mode. Rectangular shaped samples of dimension about 20 × 10 mm^2 and with a thickness in the range of 40–65 μm (measured with a digital micrometer Fischer Dualscope 603-478) were analyzed at a velocity of 1 mm/min. The mechanical parameters were obtained as the average of at least five samples.

The electrical measurements were performed in samples with the shape of plane-parallel capacitors with 5 mm diameter gold electrodes deposited on both sides of the samples with a Polaron SC502 sputter coater for good electric contact between sample and measurement equipment. The volume electrical conductivity of the samples was obtained by measuring in five places on sample the characteristic I-V curves at room temperature with a Keithley 6430 picoammeter/voltage source. The current and voltage were measured and the conductivity (σ) was calculated taken into account the geometrical factors of the samples according to:

$$\sigma = R\frac{L}{A} \tag{1}$$

where R is the electrical resistance, L is the sample thickness and A is the area of the electrodes.

Piezoresistive measurements were performed using the universal testing machine (Shimadzu model AG-IS) in 4-point-bending mode (Fig. 2). The composite was glued to a poly(propylene) board with about 1 mm thickness and gold electrodes with an area of 7 × 1.5 mm^2 were placed on the surface of the sample (Fig. 2). The electro-mechanical response was evaluated at room temperature as the average of 4 loading-unloading cycles at 5 mm/min for 0.5, 1, 1.5 and 2 mm of displacement (z).

The piezoresistive response of the composites was quantitatively evaluated by the gauge factor (GF), defined as [28]:

$$GF = \frac{\Delta R/R_0}{\Delta L/L_0} = \frac{d\rho/\rho_0}{\varepsilon} + 1 + 2\upsilon \tag{2}$$

where the R is electrical resistance, υ is Poisson coefficient, L the mechanical displacement and $\varepsilon = d\rho/\rho_0$. For the 4-point bending mode experiments, the strain was calculated from the theory of a pure bending of plates, valid between the inner loading points and given by Refs. [28,32]:

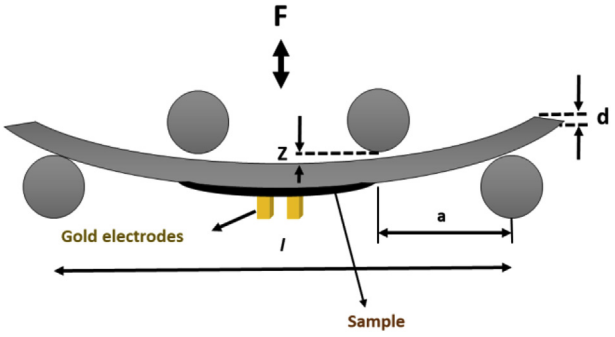

Fig. 2. Schematic representation of the 4-point bending method where z is the vertical displacement, d is the thickness of the composite/poly(propylene) stack (±1 mm), a is the distance between first and second bending points (15 mm) and l is the distance between the bending points on top of the sample ($l = 3a$).

$$\varepsilon = \frac{3dz}{5a^2} \quad (3)$$

where d, z and a correspond to the dimensions shown in Fig. 2.

3. Results and discussion

3.1. Morphological and structural properties

The BET surface areas of the carbon nanofillers varied from 35 m^2g^{-1}, obtained for G-NPL, up to 450 m^2g^{-1}, found for both GO and rGO. SWCNH showed an intermediate value of 304 m^2g^{-1}. These values are in agreement with what was reported by the suppliers.

The carbon nanofillers were also analysed by XPS. The obtained results are shown in Fig. 3 and Table 1. The spectrum obtained from G-NPL can be deconvoluted into four different peaks, namely sp^2 C=C (284.2 eV), C-OH (284.9 eV), C=O (286.9 eV) and COOH (291.3 eV), as seen in Fig. 3A [33–35]. The sp^2 peak of G-NPL is much more intense than the analogue peak of the other samples, while the other bands (C-OH, C=O and COOH) have decreased intensities, compared to those of other materials. This means that the amount of C=C is much larger in non-oxidized graphene. The oxidized materials (GO and rGO) have a higher number of

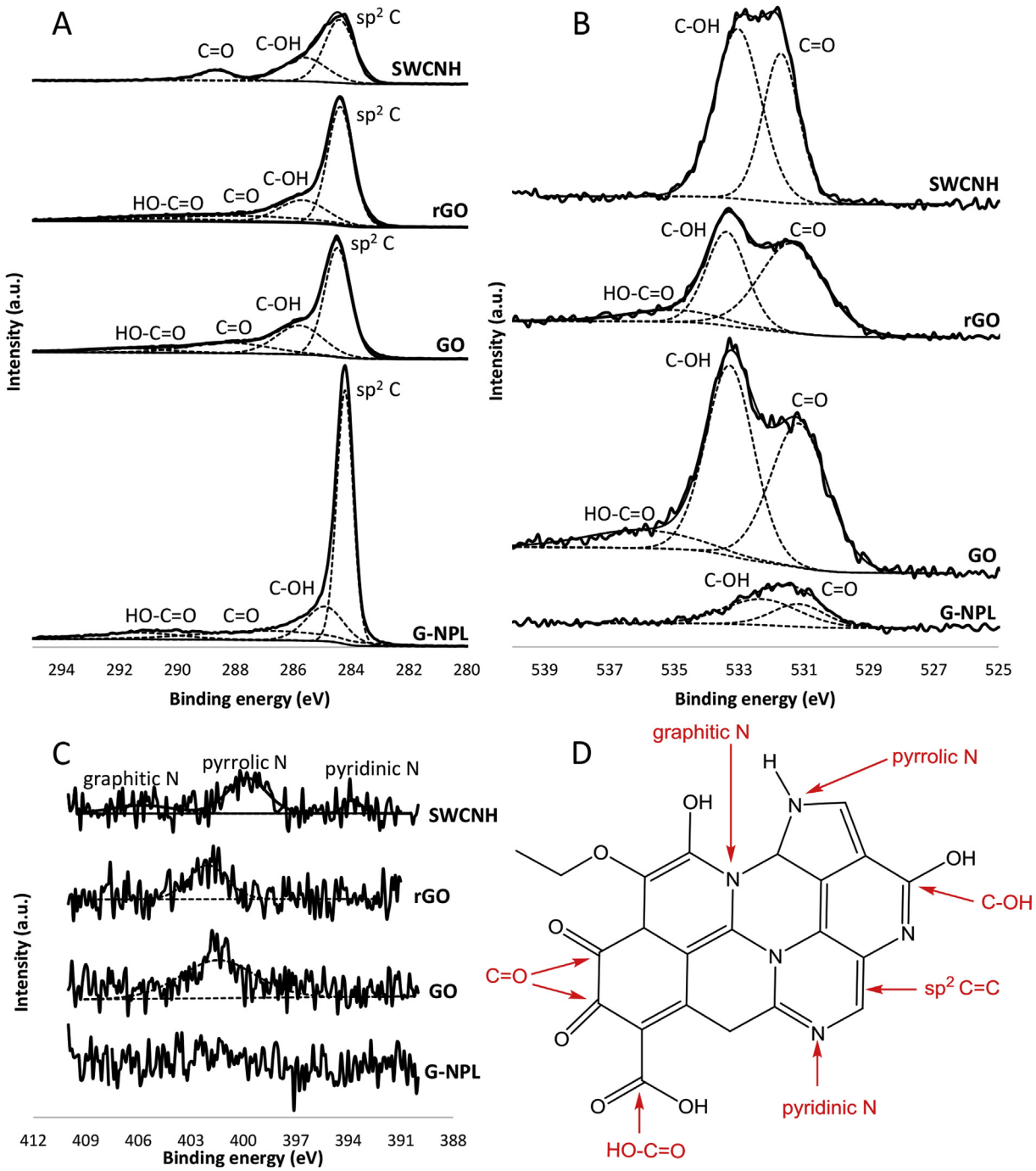

Fig. 3. XPS of carbon nanofillers: C1s (A), O1s (B) and N1s (C). (D) Schematic diagram of carbon, oxygen and nitrogen species found on graphene.

Table 1
Relative amounts (at. %) of the various elements found in the carbon nanofillers, obtained by XPS analysis.

Element	at. % G-NPL	at. % GO	at. % rGO	at. % SWCNH
C 1s	97.9	85.0	90.3	83.4
N 1s	n.d.	0.5	0.5	0.7
O 1s	2.1	14.2	8.7	15.9
S 2p	n.d.	0.3	0.5	n.d.

n.d.- not detected.

oxygenated groups, as expected. SWCNH show only three peaks that are attributed to sp^2 carbon, C-OH and C=O [36].

The O1s spectra are shown in Fig. 3B. All materials show bands at lower binding energy (attributed to C=O) and bands at slightly higher binding energy (attributed to C-OH) [34]. Interestingly, the oxidized materials (GO and rGO) also show a small band at higher binding energy, attributed to COOH [34].

The obtained N1s signals were of very low intensity and are shown in Fig. 3C. SWCNH show 3 types of N groups: graphitic (405.8 eV), pyrrolic (399.8 eV) and pyridinic (393.7 eV). A scheme of the groups is shown in Fig. 3D [34]. G-NPL show no N (or any other elements apart from C and O), evidencing the absence of impurities. GO and rGO show some peaks that are mainly attributed to pyrrolic N. However, the presence of small amounts of graphitic and pyrrolic N cannot be ruled out.

Table 1 shows that the N amount is much lower than the amount of the other elements, including that of O (as could already be derived from Fig. 3C).

The nanofillers are commercial samples and the presence of N (and S found in the graphene oxide sample) is related to procedure followed by the manufacturers (usually patent protected) to prepare the materials.

The morphology of the composites with the four different types of nanofillers is shown in the SEM surface and cross section representative images of Fig. 4. The spherulitic structure characteristic of α-PVDF is observed in Fig. 4A and B, suggesting that the carbonaceous nanofillers did not significantly influence the crystallization kinetics of the polymer [37], in the same line as reported for multi-walled carbon nanotubes (MWCNT) into PVDF [38].

The spherulites diameter is consistent with literature [39], ranging approximately from 20 to 50 μm, as can be observed in Fig. 4A and B, independently of the filler type and content, indicating that there is no modification of the crystallization kinetics, unlike other nanoparticles. Cross-section SEM images (Fig. 4C and D, respectively) show a homogeneous dispersion of the individual nanofillers, independently of the filler type and content. Further, no large agglomerated are detected in the samples.

The crystallization phase of PVDF is typically evaluated by FTIR measurements [40]. This semicrystalline polymer shows a complex structure and can present four distinct crystalline phases, but the most suitable for applications are α, β and γ-PVDF [40].

Fig. 5 shows the FTIR spectra between 600 and 1700 cm^{-1} for rGO/PVDF composites as a function of nanofiller content and the different carbonaceous nanofillers/PVDF composites with 5 wt% nanofiller.

All FTIR spectra (Fig. 5) are similar and independent of the nanofiller type and content, showing just the typical bands of α-PVDF at 614, 766, 795 and 976 cm^{-1} [40], with no traces of other phases (β or γ) being detected. Thus, the electrostatic interaction of the carbonaceous fillers with the polymer chains is not enough to promote the nucleation of the polar β or γ phases, as observed with other fillers such as ferrites or Ag [40].

The Raman spectra of the PVDF and PVDF-based composites with different carbonaceous fillers are shown in Fig. 6. The first-order Raman bands of the carbonaceous fillers are located between 1200 and 1700 cm^{-1}, while the second-order band is near 2700 cm^{-1} and can extend to 3500 cm^{-1} [41].

FLG presents four characteristic peaks observed in the Raman spectra, known as D, G, 2D and S3 bands [42]. The D found at 1350 cm^{-1} is an A_{1g} phonon corresponding to sp^2 ring-breathing mode and its intensity increases when there are defects in the edge plane of the material surface [42]. The G band, consequence of doubly degenerated vibrational mode E_{2g}, occurs at 1580 cm^{-1} [42], and it is assigned to the in-plane vibration of the sp^2-bonded carbon atoms of the hexagonal ring structure [41]. The D and G bands are observed in several carbonaceous nanofiller/PVDF composites (Fig. 6A). The Raman spectrum of G-NPL exhibits the well-known single G band at 1586 cm^{-1}, and the very weak D band at 1361 cm^{-1}, which evidences for low degree of disorder and defects

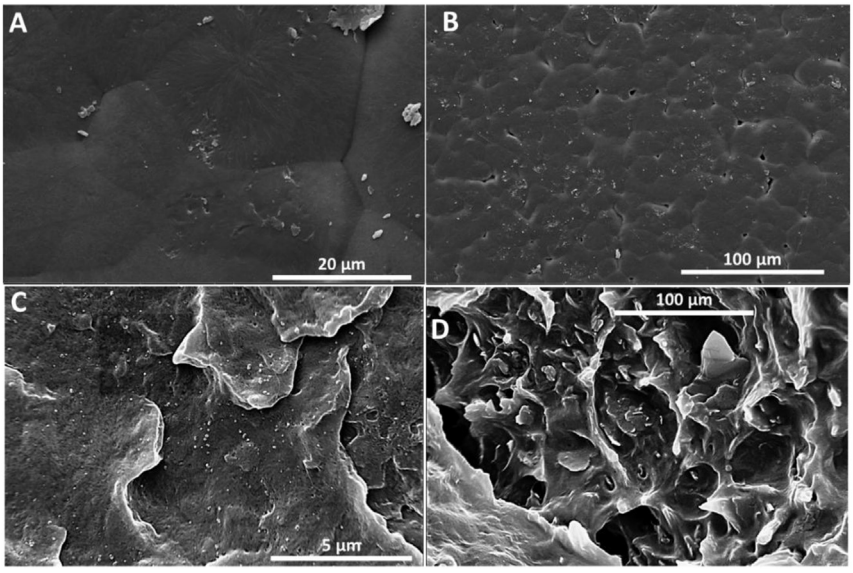

Fig. 4. SEM images of the composites with several nanofiller types and contents: A) 0.5 wt% GO; B) 0.5 wt% rGO; C) 0.5 wt% SWCNT; D) 5 wt% G-NPL. Images A) and B) are top views of the composite surfaces and C) and D) are cross-section views.

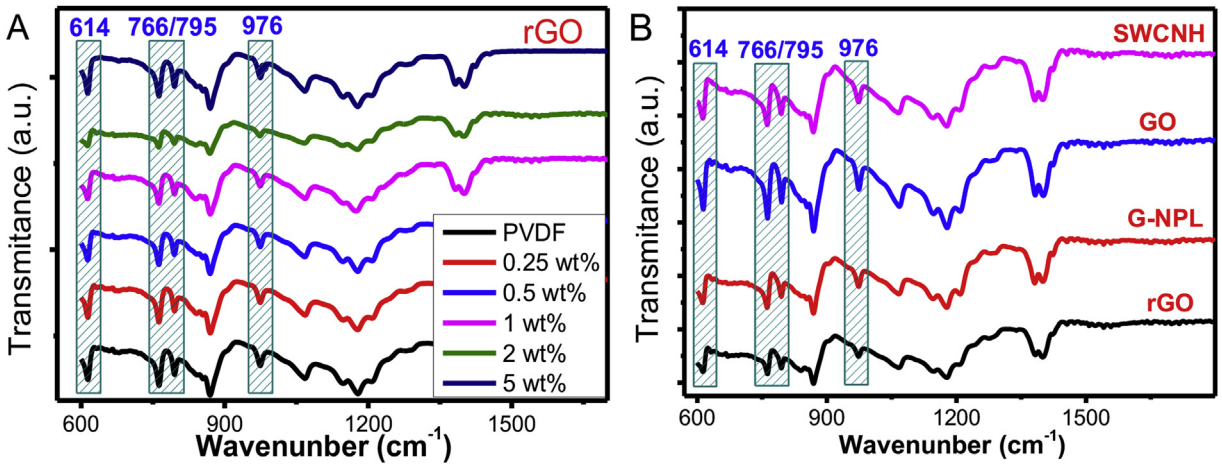

Fig. 5. FTIR spectra of A) the composite with rGO as a function of nanofiller content and B) the different composites with 5 wt% of nanofillers (SWCNH, GO, G-NPL and rGO).

in the G-NPL in the host matrix [43]. Composites containing SWCNH shows the typical D band at 1340 cm^{-1} and the G-band at 1598 cm^{-1}. The shoulder observed at 1627 cm^{-1} is assigned to the D′ band. The Raman spectra of GO and rGO present the typical spectral profile already reported for the same materials [43,44]. The 1200-1750 cm^{-1} spectral range can be deconvoluted into four main

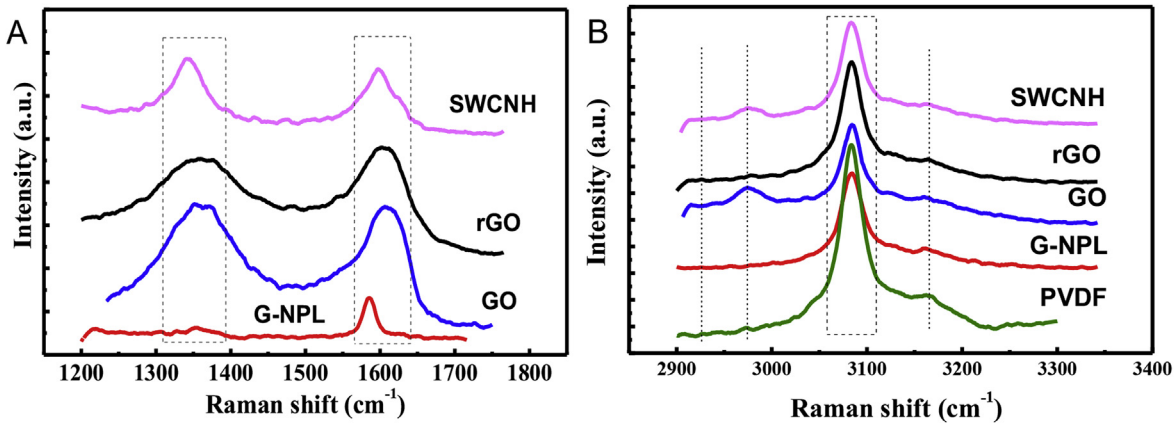

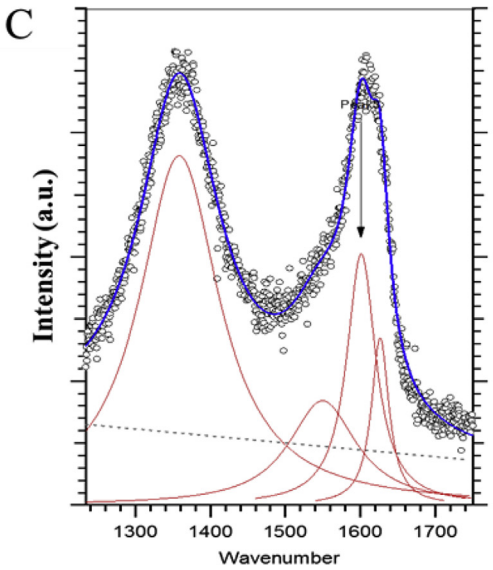

Table 2- The ratio of the bands intensity (D and G) and interdistance between defects (L_D).

	I_D / I_G	L_D (nm)
G-NPL	0.85	11
SWCNH	0.56	14
GO	1.26	9
rGO	1.61	8

Fig. 6. Raman spectra (first-order (A) and second-order transitions (B)) of PVDF composites with different FLG carbonaceous fillers (5 wt%) for GO, rGO, G-NPL and SWCNH. Deconvolution of the G band in GO into three main Raman bands (C).

Table 2
The ratio of the bands intensity (D and G) and interdistance between defects (L_D).

	I_D/I_G	L_D (nm)
G-NPL	0.85	11
SWCNH	0.56	14
GO	1.26	9
rGO	1.61	8

Raman bands, as it is shown in Fig. 6C, for the case of GO. The D band appears at 1360 cm^{-1} in both composites, while the G band locates at 1601 cm^{-1} and 1594 cm^{-1} in FLG oxide and reduced FLG oxide, respectively. In the two cases, new Raman bands are activated due to defects (D′ band) and to the finite size of graphitic crystals (D** band), pointing for a higher degree of defects in these FLG derived compounds, already ascertained by the increase of both intensity and linewidth of the D band. The upward shift of the G band peaks in composites due the PVDF fillers interaction are in agreement with the literature [45].

It is to notice taht the frequency of the D band is almost independent on the filler type. On the other hand, the G band is upshifted relatively to the G-NPL in the Raman spectra of the remaining composites, pointing for the existence of weak interactions between the nanofillers and the polymeric matrix in these composites.

The presence of the D band is a signature of defects or disorder in graphene system [41]. From the data fitting procedure, the intensity of the D (I_D) and G (I_G) bands can be determined. The lower intensity of the D band in the case of the G-NPL/PVDF composite can be related with a higher order of FLG structure of the carbonaceous nanofiller. The ratio of the intensities I_D/I_G can be used to quantify the development of disorder and defects in graphene based-systems. The ratio I_D/I_G is presented in Table 2, is calculated by equation (4). Assuming the low defect-density regime, the interdistance between defects L_D can be determined using equation [44]:

$$\frac{I_D}{I_G} = \frac{C(\lambda)}{L_D'} \tag{4}$$

where $C(\lambda) = 102\ nm^2$, for $\lambda = 514.5$ nm. The values of L_D are displayed in Table 2. The L_D value depends on the nanofiller, and increases from SWCNH/PVDF to rGO/PVDF composites, which clearly points for a decrease of defect-density in the composite series. Literature also reports that reduced states in carbon structures increase the number of aromatic domains of smaller overall size in graphene, leading to an enhancement of the I_D/I_G ratio [46].

Fig. 6B shows the Raman spectra of the PVDF and composites in the 2900-3350 cm^{-1} spectral range, where the FLG second-order bands are expected [41]. The 2D band (an overtone of the D band of graphene) is typically located around 2700 cm^{-1} and increases its intensity when the sp^2 rings are present, associated with two dimensional arbitrarily stacked FLG sheets in the c-axis [42]. This band is associated with the band structure of the FLG [42], which is not observable in our results. The second-order S3 peak (Fig. 6B), located at 2927 cm^{-1}, can be described as a product of lattice disorder and is generated from a combination of D + G bands, where FLG filler reveals by the activation of a second order band (D + G) at 2989 cm^{-1} (G-NPL), 2977 cm^{-1} (SWCNH) and 2974 cm^{-1} (GO) [42]. This band shifts up to near 2975 cm^{-1} for the composites, except for G-NPL/PVDF composite due to the lower disorder of the G-NPL structure. The α-PVDF phase presents a characteristic band near 3080 cm^{-1}, relative to CH_2 vibration frequency, and is similar for the different composites materials (Fig. 6B) [47].

The C-H stretching mode appears at 2925-2970 cm^{-1} are absorption peaks in the C-H vibration region [45]. The peak at 3160 cm^{-1} has been assigned to 2D and D + G [41].

3.2. Mechanical properties

The mechanical properties of the composites (Fig. 7) were analyzed by uniaxial stress-strain measurements until rupture of the samples. The properties of the rGO/PVDF composites as a function of the nanofillers content until 5 wt% is shown in Fig. 7A, and illustrate the typical behavior of the materials. The stress-strain data obtained from the composites with 5 wt% of the different nanofillers are presented in Fig. 7B.

The stress-strain curves of Fig. 7A show a mechanical behavior typical of a thermoplastic characterized by the elastic region with linear behavior, in which the Young's modulus is calculated (slope of stress-strain curve until 1% of deformation) and the plastic region after the yielding zone. The incorporation of the carbonaceous nanofillers into the PVDF matrices decreases the maximum strain of the composites, making them less resistant in tensile strength tests, also reported in literature [48]. The maximum strain for pristine PVDF ranges between 16 and 18%, whereas it ranges between 2 and 5% for the various composites. The Young's modulus of pristine PVDF is 1.16 ± 0.03 GPa and the values obtained for the

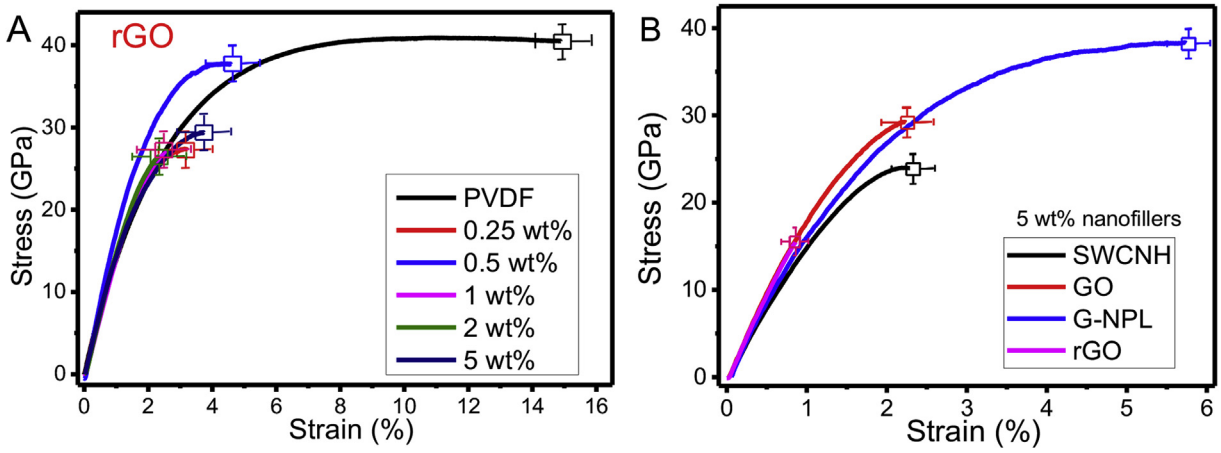

Fig. 7. Stress-strain mechanical curve measurements at 1 mm/min as a function of nanofillers type and content for A) rGO composites and B) composites with 5 wt% carbonaceous nanofillers (SWCNH, GO, G-NPL and rGO).

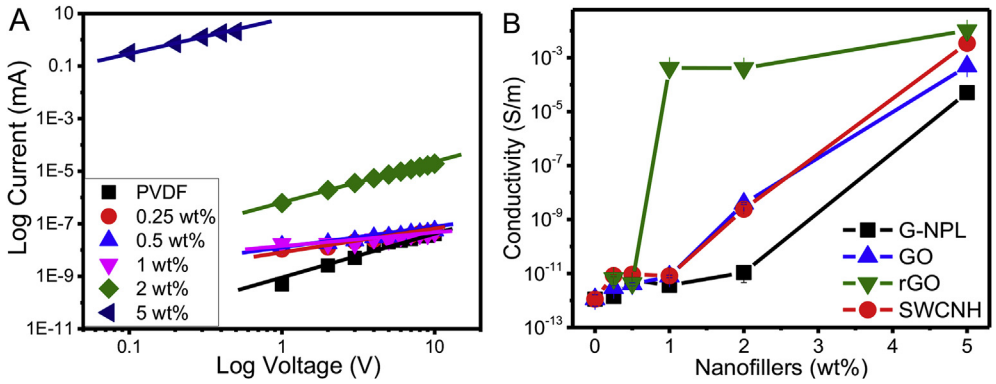

Fig. 8. Current/voltage curves for A) SWCNH/PVDF composites up to 5 wt.% SWCNH and B) electrical conductivity as a function of nanofiller content for the composites with G-NPL, GO, rGO and SWCNH.

composites are similar among different samples ranging between (1.10–1.70) ± 0.03 GPa, presenting an increasing trend with nanofiller content increase up to 5 wt%. The maximum stress is about 40 GPa for the pristine PVDF sample, whereas the composites generally present lower values, decreasing with increase of nanofiller content, reaching a minimum of about 25 GPa for the sample with 5 wt% SWCNH. Although the SEM images in Fig. 4C and D show good nanofiller dispersion and interface between polymer and nanofillers, the samples with increased nanofiller contents become ductile. Raman results shows no robust connection between PVDF and several carbonaceous nanofillers. The composites with higher L_D show larger maximum strain compared to the ones with lower distance defects material, rGO. This effect could also be observed in CNT/PVDF composites after percolation threshold, where the maximum strain and strength decreased for materials up to 3 wt% CNT [49]. For composites after the percolation threshold, the interconnection points between the nanofiller (e.g. CNT) might not allow transmitting efficiently loads between the components of the nanocomposite reducing the Young's modulus in the materials [49].

3.3. Electrical properties

The current/voltage curves obtained from SWCNH/PVDF composites (Fig. 8A) and electrical behavior of the nanofillers/PVDF composites for different nanofillers (Fig. 8B) and content was evaluated by measuring the bulk electrical conductivity. The electrical conductivity for α-PVDF is around 5.0×10^{-12} S/m and increases with nanofiller content increase for the composites with a percolative behavior similar to that found for other carbonaceous nanofillers/PVDF composites, such as SWCNT [50] and MWCNT [51,52]. The maximum conductivity was obtained for 5 wt% SWCNH and rGO nanofillers near 0.01 S/m (Fig. 8B).

The electrical conductivity increases in composites with increasing carbonaceous nanofiller content. Nevertheless, there are strong differences between the different nanofillers, which indicates that their behavior depends on the intrinsic properties of the carbon materials, since the preparation method, polymer matrix and content is the same for all composite samples.

Use of the rGO nanofiller results in a higher electrical conductivity for composites with contents larger than 0.5 wt%. rGO/PVDF composites show an electrical percolation threshold (PT) between 0.5 and 1 wt% of nanofillers, with electrical conductivity $\sigma \approx 0.01$ S/m for the material with 5 wt%. Oxided FLG materials increase the electrical conductivity of the composites, mainly the rGO, as reported in the literature [53,54]. The remaining nanofillers present larger percolation threshold compared to rGO, around 2 wt% for GO and SWCNH and larger for the G-NPL nanofillers. Larger thickness of the G-NPL nanofillers decrease their electrical properties in composites. The maximum conductivity (obtained for composites with 5 wt% of nanofillers) of $\sigma \approx 1 \times 10^{-2}$ S/m is highest for rGO, and lowest at $\sigma \approx 1 \times 10^{-4}$ S/m for G-NPL nanofillers. The electrical conductivity and geometry of the nanofillers influence the percolation threshold and maximum conductivity of the composite materials. The reduction process applied to FLG oxide (to obtain rGO) greatly improves their electrical conductivity, that can increase up to 6 orders of magnitude, when compared to GO [55]. In this way, composites with rGO present a lower percolation threshold in polymer composites, as can be observed in Fig. 8B. Composite with SWCNH have a similar behavior to GO nanofillers. It has been reported that lower aspect ratio (AR ≈ 10) of the SWCNH (30–50 nm of length and 3–5 nm of diameter) decreases the percolation threshold [8], although the electrical conductivity can be higher compared to GO nanofillers (high purity material) and their geometry increases the percolation threshold. G-NPL nanofillers present similar geometry and dimensions compared to GO and rGO, but show lower conductivity among all nanofiller contents due to their homogeneous dispersion in polymer composites and large size G-NPL aggregates that can be observed [56]. Although the G-NPL (and also SWCNH) shows, by XPS or Raman, which contains lower oxide groups and defects in the edge plan in their surface their intrinsic electrical properties have less influence than geometrical properties in carbonaceous nanofiller/PVDF

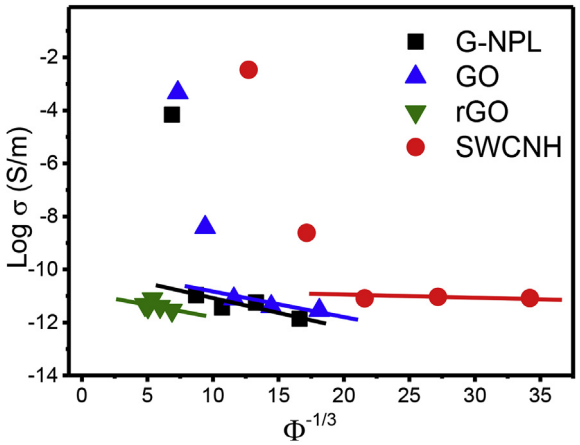

Fig. 9. Logarithmic plot of the conductivity (σ) as a function of the volume fraction ($\Phi^{-1/3}$) for the different nanofillers/PVDF composites for G-NPL, GO, rGO and SWCNH up to 5 wt% of nanofillers.

composites.

In order to get some hints on the theoretical electric conduction mechanism, Fig. 9 shows the linear relation between the logarithm of the conductivity and the filler content for several volume fractions of the nanofillers in the different composite types. The volume fractions (Φ) are calculated based on the mass weight of the composites and density of the carbon nanofillers.

Fig. 9 shows that the electrical conductivity follows a $\log(\sigma) \propto \Phi^{-1/3}$ linear relationship after the percolation threshold. This type of relation appears when the conductivity is due to hopping between nearest neighbors (nanofillers) that form a conductive network [57]. This linear relation also appears in related composite systems, based on conductive fillers embedded in polymer matrices, such as CNT [38,57].

Another important issue is the effect of the oxidation, which delays the percolation threshold due to the surface modification of the filler that reduces their conductivity. This effect has been reported previously for CNT/PVDF composites [38].

3.4. Electro-mechanical properties

The piezoresistive properties of several conductive nanofillers/PVDF composites are presented in Fig. 10, for different nanofiller types and sample displacements. The results are representative for the other composites. The electro-mechancial properties were measured in composites with 5 wt% nanofiller content due to the lower electrical conductivity of GO and SWCNH composites for lower nanofiller contents. Although piezoresistive sensibility is typically higher near the percolation threshold, the deformation region for linear piezoresistive reponse is low, mainly due to the breakdown of the conductive network within the composite [58]. For a larger deformation region of linear response between electrical resistance variation and mechancial stress, which is required for large deformation strain sensor, larger fillers contents are required [58]. The G-NPL nanofillers in composite with 5 wt% do not show piezoresistive properties due to their between 1 and 3 orders of magnitude lower electrical conductivity for the contents used in the composites. Materials with larger electrical resistance do not present linear correlation between the resistance and the mechanical stimulus.

The piezoresistive measurements in 4-point-bending mode were performed from 0.5 to 2 mm of vertical displacement (z direction in Fig. 2) in three different composites with 5 wt% of nanofillers (SWCNH, GO and rGO). Fig. 10 shows representative examples for the different composites and displacements.

Fig. 10 shows the electro-mechanical behavior of the composites, where the relative electrical resistance increases with increasing strain applied to the composites and decreases when the strainis reduced towards the initial point (i.e., zero displacement). This behavior is similar for different composites and displacements. The piezoresistive sensibility of the composites was evaluated by the respective gauge factor (GF) and is represented in Fig. 11. The

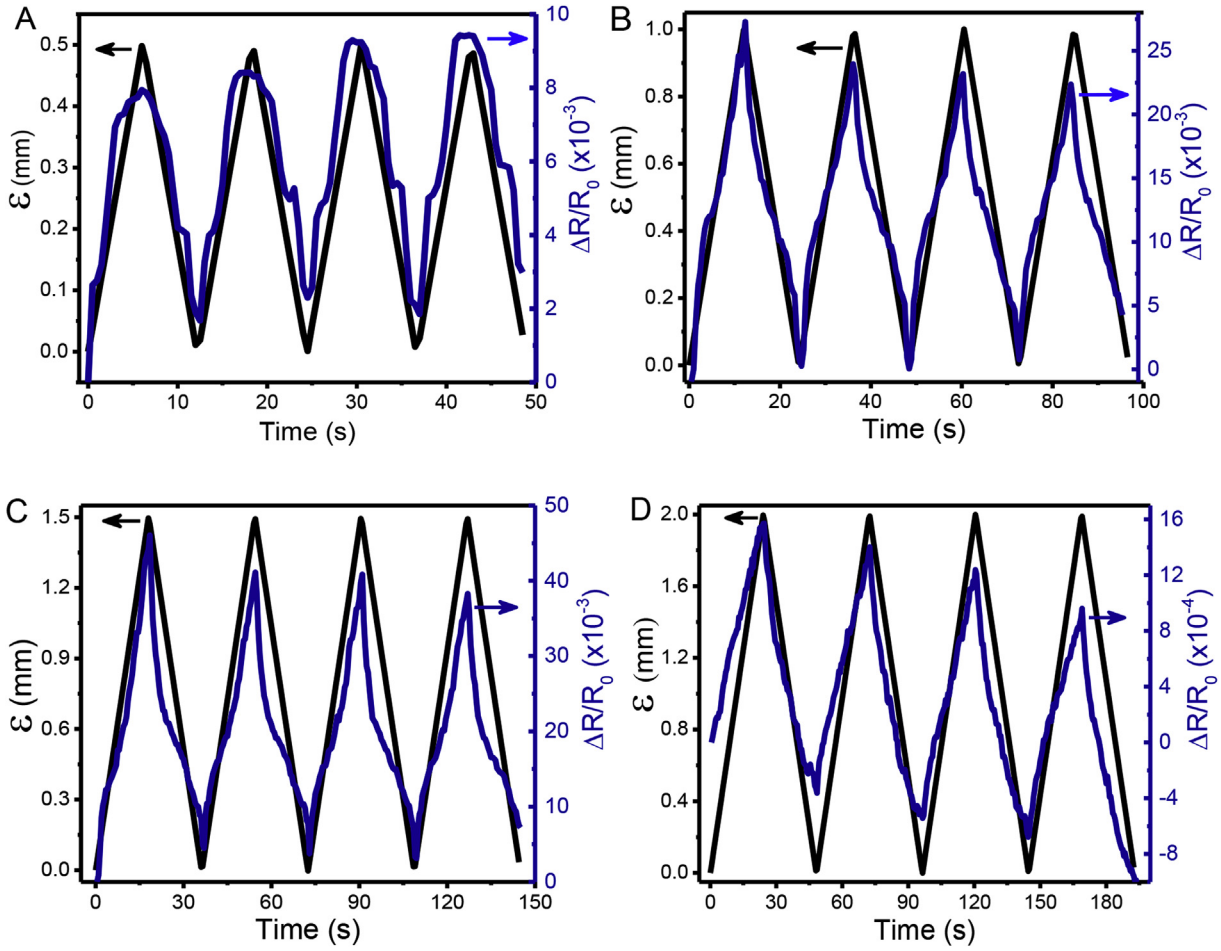

Fig. 10. Representative piezoresistive measurements of nanofillers/PVDF composites with 5 wt.% nanofiller content and for different displacements: A) GO for 0.5 mm; rGO for B) 1 mm and C) 1.5 mm; D) SWCNH for 2 mm.

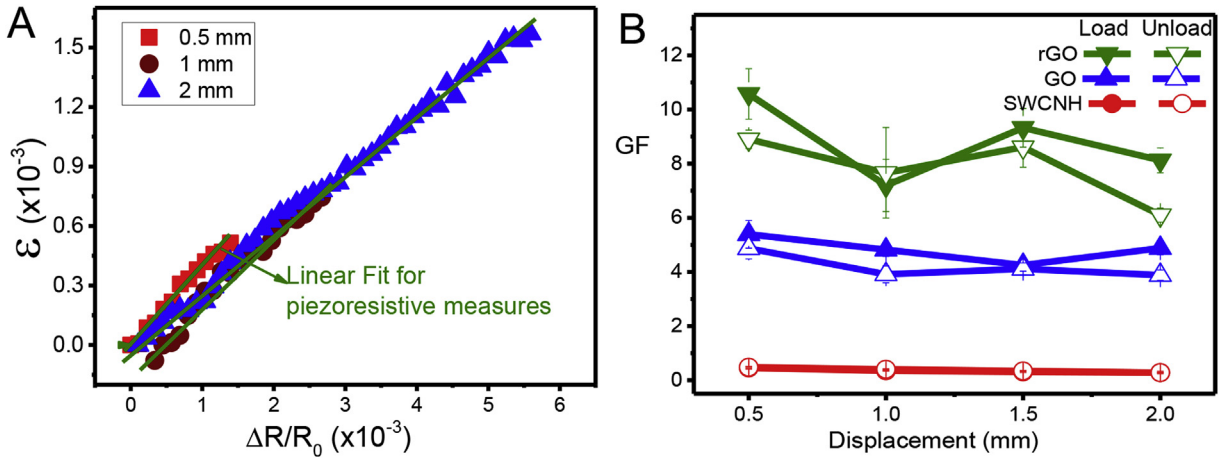

Fig. 11. Piezoresistive sensibility (GF) measurements: A) exemplification for 0.5, 1 and mm for rGO sample and B) for composites with 5 wt% of nanofillers applying 0.5–2 mm of displacement at 5 mm/min.

linear correlation between electrical resistance variation with mechanical stress applied to the composites is observed in Fig. 11A for several deformations (0.5, 1 and 2 mm), with respective piezoresistive sensibility in Fig. 11B for the different carbon nanofiller materials.

The electro-mechanical behavior depends on the nanofiller present in the composites, rGO showing the largest GF values and SWCNH the lowest ones. SWCNH show GF ≈ 0.5 for loading and unloading mechanical cycles. The composite with 5 wt% of GO presents a GF varying from about 4 to 6. The larger GF values (i.e., from 7 to 11) were obtained for rGO-based composites, applying 1 and 0.5 mm displacement, respectively. Use of the FLG (oxide and reduced) nanofillers results in larger piezoresistive sensibility than SWCNH. The geometry thus influences the electrical conductivity and piezoresistive properties, since both graphene oxide nanofillers have a diameter of 1–5 μm and a thickness of only few nm (AR ≈ 1000), whereas SWCNH have AR ≈ 10. Literature reports that FLG can have higher sensibility than CNT in PDMS composites [27].

The piezoresistive response has two contributions (equation (3)), intrinsic piezoresistive effect $((d\rho/\rho_0)/\varepsilon)$ and geometrical effect $(1+2\upsilon)$ [28]. The geometric effect depends on the Poisson coefficient and the maximum value of the GF contributions is 2 (with $\upsilon = 0.5$) for incompressible materials [59]. Piezoresistive composites with larger GF values than their geometric factor present intrinsic conductivity variation when stress is applied on the composites. GO and rGO in composite with 5 wt% nanofiller content show intrinsic electrical conductivity variation in piezoresistive measurements. The polymer matrices can influence their properties [60,61], but these composites were prepared with same polymer in similar conditions. The conductive and geometric properties of the nanofillers (such as length and diameter) influence the overall properties of the composites, as well as their piezoresistive sensibility [62]. The nanofillers with larger diameter show higher piezoresistive sensibility. In the case of SWCNH, GF ≈ 0.5 and their diameter is 1000 times smaller than that of the remaining nanofillers. Given the specific diameter and length of the SWCNH a significantly lower AR is reached compared to the treated FLG nanofillers. Aspect ratio influences the electrical properties (percolation threshold) of the composites and the piezoresistive sensibility [58]. The electro-mechanical behavior is similar for different composites, but the piezoresistive sensibility depends on the geometry of the nanofillers [58]. On the other hand, piezoresistive sensibility can be modified by adding a second filler to the polymer-based composites or aligning the conductive nanofillers during proccesing [63–65]. Thus, higher piezoresistive sensibility has been shown in ternary composites as a result of inducing the breakup of the conductive network by a second filler [63] or by aligning multiwalled CNTs [64].

4. Conclusions

Composites based on PVDF with different nanocarbon allotropes were prepared by solvent casting. The composite samples crystallized in the compact and spherulitic morphology of α-PVDF with the carbonaceous nanofillers well dispersed and distributed along the polymer matrix. XPS shows that oxidation process in creates larger number of oxide groups in GO an rGO nanofillers. Raman analysis presents the FLG bands in the composites, with G-NPL nanofiller showing a lower intensity D band and thus lower content of FLG defects, being similar for remain nanofillers. Composites showed stretchability up to ≈5% compared to 15% of the PVDF polymer. The conductivity follows a percolate behavior increasing with nanofiller content increase, achieving a maximum of ~0.01 $(\Omega\ m)^{-1}$ for the rGO/PVDF with 5 wt% filler content, nine orders of magnitude higher than pure PVDF sample. The percolation threshold is lower than 1 wt% nanofiller for rGO composites, and similar (i.e., about 2 wt% nanofiller content) for the remaining composites. The main conductivity mechanism is hopping between the nearest neighbors (nanofillers) that form a conductive network in composites.

Due to their electrical properties, rGO/PVDF, GO/PVDF and SWCNH/PVDF composites present piezoresistive properties unlike the sample of 5 wt% G-NPL/PVDF. Composites with 5 wt% nanofiller show GF values ranging between about 0.5 and 11 for displacements between 0.5 and 2 mm. The rGO/PVDF composite shows highest GF values (i.e., between about 7 and 11) for all deformations. Thus, it is shown that the geometry of the carbonaceous nanofillers influences the piezoresistive sensibility, with FLG shapes with larger AR showing larger GF values compared to SWCNH, which shows the lowest AR. Reduced FLG oxide leads to a lower percolation threshold and larger GF values in the PVDF composites. In conclusion, this study demonstrates that conductive of the carbonaceous nanofillers allow to tune the electro-mechanical properties of the composites, depending on their physico-chemical properties, being suitable candidates for strain sensing applications.

Acknowledgements

This work was supported by the Portuguese Foundation for Science and Technology (FCT) in the framework of the Strategic Funding UID/FIS/04650/2013, project PTDC/EEI-SII/5582/2014, grants SFRH/BPD/110914/2015 and SFRH/BD/98219/2013 (P.C. and J.O., respectively), as well POCH and European Union. J.N.P. wish to thank the financial support of the project Centro-01-0145-FEDER-000017 - EMaDeS - Energy, Materials and Sustainable Development, co-financed by the Portugal 2020 Program (PT 2020), within the Regional Operational Program of the Center (CENTRO 2020) and the European Union through the European Regional Development Fund (ERDF). The authors acknowledge funding by the Spanish Ministry of Economy and Competitiveness (MINECO) through the project MAT2016-76039-C4-3-R (AEI/FEDER, UE) and from the Basque Government Industry Department under the ELKARTEK program. SACC acknowledges Fundação para a Ciência e a Tecnologia (FCT) for Investigador FCT program (IF/01381/2013/CP1160/CT0007) and Project POCI-01-0145-FEDER-006984—Associate Laboratory LSRE-LCM funded by FEDER through COMPETE2020—POCI and by FCT. Authors are thankful to Dr Carlos M. Sá (CEMUP) for assistance with XPS analyses.

Appendix A. Supplementary data

Supplementary data related to this article can be found at https://doi.org/10.1016/j.compscitech.2017.11.001.

References

[1] R. Simoes, J. Silva, R. Vaia, V. Sencadas, P. Costa, J. Gomes, S. Lanceros-Mendez, Low percolation transitions in carbon nanotube networks dispersed in a polymer matrix: dielectric properties, simulations and experiments, Nanotechnology 20 (3) (2009) 035703.
[2] M. Amjadi, K.-U. Kyung, I. Park, M. Sitti, Stretchable skin-mountable, and wearable strain sensors and their potential applications: a review, Adv. Funct. Mater. 26 (11) (2016) 1678–1698.
[3] D.J. Bergman, D. Stroud, Physical-properties of macroscopically inhomogeneous-media, Solid State Phys. 46 (1992) 147–269.
[4] C. Brosseau, P. Queffelec, P. Talbot, Microwave characterization of filled polymers, J. Appl. Phys. 89 (8) (2001) 4532–4540.
[5] Y.H. Cheng, X.L. Chen, K. Wu, S.N. Wu, Y. Chen, Y.M. Meng, Modeling and simulation for effective permittivity of two-phase disordered composites, J. Appl. Phys. 103 (3) (2008) 034111.
[6] Y.K. Yang, C.P. Han, B.B. Jiang, J. Iocozzia, C.G. He, D. Shi, T. Jiang, Z.Q. Lin, Graphene-based materials with tailored nanostructures for energy conversion and storage, Mat. Sci. Eng. R. 102 (2016) 1–72.
[7] J. Nunes-Pereira, A.R. Silva, C. Ribeiro, S.A.C. Carabineiro, J.G. Buijnsters, S. Lanceros-Mendez, Nanodiamonds/poly(vinylidene fluoride) composites for tissue engineering applications, Compos Part B-Eng 111 (2017) 37–44.
[8] H. Deng, L. Lin, M.Z. Ji, S.M. Zhang, M.B. Yang, Q. Fu, Progress on the morphological control of conductive network in conductive polymer composites and the use as electroactive multifunctional materials, Prog. Polym. Sci. 39 (4) (2014) 627–655.
[9] P. Costa, J. Silva, V. Sencadas, C.M. Costa, F.W.J. van Hattum, J.G. Rocha, S. Lanceros-Mendez, The effect of fibre concentration on the α to β-phase transformation, degree of crystallinity and electrical properties of vapour grown carbon nanofibre/poly(vinylidene fluoride) composites, Carbon 47 (11) (2009) 2590–2599.
[10] J.Z. Xu, G.J. Zhong, B.S. Hsiao, Q. Fu, Z.M. Li, Low-dimensional carbonaceous nanofiller induced polymer crystallization, Prog. Polym. Sci. 39 (3) (2014) 555–593.
[11] K.K. Sadasivuni, D. Ponnamma, S. Thomas, Y. Grohens, Evolution from graphite to graphene elastomer composites, Prog. Polym. Sci. 39 (4) (2014) 749–780.
[12] D.-X. Yan, H. Pang, B. Li, R. Vajtai, L. Xu, P.-G. Ren, J.-H. Wang, Z.-M. Li, Structured reduced graphene oxide/polymer composites for ultra-efficient electromagnetic interference shielding, Adv. Funct. Mater. 25 (4) (2015) 559–566.
[13] P. Jojibabu, M. Jagannatham, P. Haridoss, G.D.J. Ram, A.P. Deshpande, S.R. Bakshi, Effect of different carbon nano-fillers on rheological properties and lap shear strength of epoxy adhesive joints, Compos Part a-Appl S 82 (2016) 53–64.
[14] H. Pang, L. Xu, D.X. Yan, Z.M. Li, Conductive polymer composites with segregated structures, Prog. Polym. Sci. 39 (11) (2014) 1908–1933.
[15] B.F. Gonçalves, P. Costa, J. Oliveira, S. Ribeiro, V. Correia, G. Botelho, S. Lanceros-Mendez, Green solvent approach for printable large deformation thermoplastic elastomer based piezoresistive sensors and their suitability for biomedical applications, J. Polym. Sci. Part B Polym. Phys. 54 (20) (2016) 2092–2103.
[16] Z. Spitalsky, D. Tasis, K. Papagelis, C. Galiotis, Carbon nanotube-polymer composites: chemistry, processing, mechanical and electrical properties, Prog. Polym. Sci. 35 (3) (2010) 357–401.
[17] J. Silva, S. Lanceros-Mendez, R. Simoes, Effect of cylindrical filler aggregation on the electrical conductivity of composites, Phys. Lett. A 378 (40) (2014) 2985–2988.
[18] N. Hu, T. Itoi, T. Akagi, T. Kojima, J.M. Xue, C. Yan, S. Atobe, H. Fukunaga, W.F. Yuan, H.M. Ning, Surina, Y.L. Liu, Alamusi, Ultrasensitive strain sensors made from metal-coated carbon nanofiller/epoxy composites, Carbon 51 (2013) 202–212.
[19] P. Wang, S.N. Geng, T.H. Ding, Effects of carboxyl radical on electrical resistance of multi-walled carbon nanotube filled silicone rubber composite under pressure, Compos Sci. Technol. 70 (10) (2010) 1571–1573.
[20] B. Nigro, C. Grimaldi, M.A. Miller, P. Ryser, T. Schilling, Tunneling conductivity in composites of attractive colloids, J. Chem. Phys. 136 (16) (2012) 164903.
[21] H. Zhu, X. Wang, J. Liang, H. Lv, H. Tong, L. Ma, Y. Hu, G. Zhu, T. Zhang, Z. Tie, Z. Liu, Q. Li, L. Chen, J. Liu, Z. Jin, Versatile electronic skins for motion detection of joints enabled by aligned few-walled carbon nanotubes in flexible polymer composites, Adv. Funct. Mater. 27 (21) (2017) 1606604. -n/a.
[22] T.T. Tung, C. Robert, M. Castro, J.F. Feller, T.Y. Kim, K.S. Suh, Enhancing the sensitivity of graphene/polyurethane nanocomposite flexible piezo-resistive pressure sensors with magnetite nano-spacers, Carbon 108 (2016) 450–460.
[23] S.W. Sun, B.G. Han, S. Jiang, X. Yu, Y.L. Wang, H.Y. Li, J.P. Ou, Nano graphite platelets-enabled piezoresistive cementitious composites for structural health monitoring, Constr. Build. Mater 136 (2017) 314–328.
[24] K. Nasouri, A.M. Shoushtari, Designing, modeling and manufacturing of lightweight carbon nanotubes/polymer composite nanofibers for electromagnetic interference shielding application, Compos Sci. Technol. 145 (2017) 46–54.
[25] R.K. Layek, A.K. Das, M.J. Park, N.H. Kim, J.H. Lee, Enhancement of physical, mechanical, and gas barrier properties in noncovalently functionalized graphene oxide/poly(vinylidene fluoride) composites, Carbon 81 (2015) 329–338.
[26] S.J. Benight, C. Wang, J.B.H. Tok, Z.A. Bao, Stretchable and self-healing polymers and devices for electronic skin, Prog. Polym. Sci. 38 (12) (2013) 1961–1977.
[27] A. Nakamura, T. Hamanishi, S. Kawakami, M. Takeda, A piezo-resistive graphene strain sensor with a hollow cylindrical geometry, Mater Sci. Eng. B-Adv 219 (2017) 20–27.
[28] P. Costa, A. Ferreira, V. Sencadas, J.C. Viana, S. Lanceros-Mendez, Electro-mechanical properties of triblock copolymer styrene-butadiene-styrene/carbon nanotube composites for large deformation sensor applications, Sens. Actuat a-Phys 201 (2013) 458–467.
[29] H.C. Bidsorkhi, A.G. D'Aloia, G. De Bellis, A. Proietti, A. Rinaldi, M. Fortunato, P. Ballirano, M.P. Bracciale, M.L. Santarelli, M.S. Sarto, Nucleation effect of unmodified graphene nanoplatelets on PVDF/GNP film composites, Mater. Today Commun. 11 (2017) 163–173.
[30] J.M.M.M. de Almeida, J.A. Moreira, Influence of diffusion parameters on the spectral characteristics of raman modes of titanium-diffused lithium niobate planar waveguides, Spectrosc. Lett. 46 (6) (2013) 453–458.
[31] S. Brunauer, P.H. Emmett, E. Teller, Adsorption of gases in multimolecular layers, J. Am. Chem. Soc. 60 (2) (1938) 309–319.
[32] A. Ferreira, M.T. Martínez, A. Ansón-Casaos, L.E. Gómez-Pineda, F. Vaz, S. Lanceros-Mendez, Relationship between electromechanical response and percolation threshold in carbon nanotube/poly(vinylidene fluoride) composites, Carbon 61 (Supplement C) (2013) 568–576.
[33] H.P. Cong, X.C. Ren, P. Wang, S.H. Yu, Flexible graphene-polyaniline composite paper for high-performance supercapacitor, Energ Environ. Sci. 6 (4) (2013) 1185–1191.
[34] L. Zheng, Y. Chang, F. Xiaoming, L. Shaohong, Y. Juan, Z. Mengdi, W. Gang, X. Nan, Q. Jieshan, Freeze-drying for sustainable synthesis of nitrogen doped porous carbon cryogel with enhanced supercapacitor and lithium ion storage performance, Nanotechnology 26 (37) (2015) 374003.
[35] S. Park, J. An, I. Jung, R.D. Piner, S.J. An, X. Li, A. Velamakanni, R.S. Ruoff, Colloidal suspensions of highly reduced graphene oxide in a wide variety of organic solvents, Nano Lett. 9 (4) (2009) 1593–1597.
[36] A.B. Deshmukh, M.V. Shelke, Synthesis and electrochemical performance of a single walled carbon nanohorn-Fe3O4 nanocomposite supercapacitor electrode, Rsc Adv. 3 (44) (2013) 21390–21393.
[37] R. Gregorio, R.C. Capitao, Morphology and phase transition of high melt temperature crystallized poly(vinylidene fluoride), J. Mater Sci. 35 (2) (2000) 299–306.
[38] S.A.C. Carabineiro, M.F.R. Pereira, J. Nunes-Pereira, J. Silva, C. Caparros, V. Sencadas, S. Lanceros-Mendez, The effect of nanotube surface oxidation on the electrical properties of multiwall carbon nanotube/poly(vinylidene fluoride) composites, J. Mater Sci. 47 (23) (2012) 8103–8111.
[39] M.P. Silva, V. Sencadas, G. Botelho, A.V. Machado, A.G. Rolo, J.G. Rocha, S. Lanceros-Mendez, α-, γ-PVDF: crystallization kinetics, microstructural variations and thermal behaviour, Mater. Chem. Phys. 122 (1) (2010) 87–92.
[40] P. Martins, A.C. Lopes, S. Lanceros-Mendez, Electroactive phases of

poly(vinylidene fluoride): determination, processing and applications, Prog. Polym. Sci. 39 (4) (2014) 683–706.
[41] S.K. Sze, N. Siddique, J.J. Sloan, R. Escribano, Raman spectroscopic characterization of carbonaceous aerosols, Atmos. Environ. 35 (3) (2001) 561–568.
[42] G. Xu, N. Aydemir, P.A. Kilmartin, J. Travas-Sejdic, Direct laser scribed graphene/PVDF-HFP composite electrodes with improved mechanical water wear and their electrochemistry, Appl. Mater. Today 8 (2017) 35–43.
[43] K.N. Kudin, B. Ozbas, H.C. Schniepp, R.K. Prud'homme, I.A. Aksay, R. Car, Raman spectra of graphite oxide and functionalized graphene sheets, Nano Lett. 8 (1) (2008) 36–41.
[44] A. Kaniyoor, S. Ramaprabhu, A Raman spectroscopic investigation of graphite oxide derived graphene, Aip Adv. 2 (3) (2012) 032183.
[45] I.S. Elashmawi, L.H. Gaabour, Raman, morphology and electrical behavior of nanocomposites based on PEO/PVDF with multi-walled carbon nanotubes, Results Phys. 5 (2015) 105–110.
[46] X. Zhao, Q. Zhang, D. Chen, P. Lu, Enhanced mechanical properties of graphene-based poly(vinyl alcohol) composites, Macromolecules 43 (5) (2010) 2357–2363.
[47] N.J. Ramer, T. Marrone, K.A. Stiso, Structure and vibrational frequency determination for α-poly(vinylidene fluoride) using density-functional theory, Polymer 47 (20) (2006) 7160–7165.
[48] J. Liang, Y. Huang, L. Zhang, Y. Wang, Y. Ma, T. Guo, Y. Chen, Molecular-level dispersion of graphene into poly(vinyl alcohol) and effective reinforcement of their nanocomposites, Adv. Funct. Mater. 19 (14) (2009) 2297–2302.
[49] F.A. Sanchez, J. Gonzalez-Benito, PVDFBaTiO3/Carbon nanotubes ternary nanocomposites: effect of nanofillers and processing, Polym. Compos. 38 (2) (2017) 227–235.
[50] A. Ansón-Casaos, J.M. González-Domínguez, A.M. Díez-Pascual, M.A. Gómez-Fatou, M.T. Martínez, Choosing the chemical route for carbon nanotube integration in poly(vinylidene fluoride), J. Phys. Chem. C 116 (30) (2012) 16217–16225.
[51] H. Wang, K. Zheng, X. Zhang, T.X. Du, C. Xiao, X. Ding, C. Bao, L. Chen, X.Y. Tian, Segregated poly(vinylidene fluoride)/MWCNTs composites for high-performance electromagnetic interference shielding, Compos Part a-Appl S 90 (2016) 606–613.
[52] S. Begum, A. Kausar, H. Ullah, M. Siddiq, Potential of polyvinylidene fluoride/carbon nanotube composite in energy, electronics, and membrane Technology: an overview, Polym-Plast Technol. 55 (18) (2016) 1949–1970.
[53] J.R. Potts, D.R. Dreyer, C.W. Bielawski, R.S. Ruoff, Graphene-based polymer nanocomposites, Polymer 52 (1) (2011) 5–25.
[54] R. Atif, I. Shyha, F. Inam, Mechanical, thermal, and electrical properties of graphene-epoxy nanocomposites-A review, Polymers 8 (8) (2016).
[55] M.Z.B. Dzukarnain, T. Takami, H. Imai, T. Ogino, Highly conductive, monolayer and large-area reduced graphene oxide films fabricated by electrical connection at the two-dimensional boundaries between the tiled graphene oxide flakes, Thin Solid Films 615 (2016) 247–255.
[56] L. Yue, G. Pircheraghi, S.A. Monemian, I. Manas-Zloczower, Epoxy composites with carbon nanotubes and graphene nanoplatelets - dispersion and synergy effects, Carbon 78 (2014) 268–278.
[57] J. Silva, R. Simoes, S. Lanceros-Mendez, R. Vaia, Applying complex network theory to the understanding of high-aspect-ratio carbon-filled composites, Epl-Europhys Lett. 93 (3) (2011) 37005.
[58] N. Alamusi, H. Hu, S. Fukunaga, Atobe, Y. Liu, J. Li, Piezoresistive strain sensors made from carbon nanotubes based polymer nanocomposites, Sensors Basel, Switz. 11 (11) (2011) 10691–10723.
[59] A. Vinogradov, F. Holloway, Electro-mechanical properties of the piezoelectric polymer PVDF, Ferroelectrics 226 (1–4) (1999) 169–181.
[60] P. Costa, S. Ribeiro, S. Lanceros-Mendez, Mechanical vs. electrical hysteresis of carbon nanotube/styrene-butadiene-styrene composites and their influence in the electromechanical response, Compos Sci. Technol. 109 (2015) 1–5.
[61] H.A.K. Toprakci, S.K. Kalanadhabhatla, R.J. Spontak, T.K. Ghosh, Polymer nanocomposites containing carbon nanofibers as soft printable sensors exhibiting strain-reversible piezoresistivity, Adv. Funct. Mater. 23 (44) (2013) 5536–5542.
[62] E. Falletta, P. Costa, C. Della Pina, S. Lanceros-Mendez, Development of high sensitive polyaniline based piezoresistive films by conventional and green chemistry approaches, Sens. Actuat a-Phys 220 (0) (2014) 13–21.
[63] J.W. Zha, W.K. Li, J. Zhang, C.Y. Shi, Z.M. Dang, Influence of the second filler on the positive piezoresistance behavior of carbon nanotubes/silicone rubber composites, Mater Lett. 118 (2014) 161–164.
[64] A.I. Oliva-Avilés, F. Avilés, V. Sosa, Electrical and piezoresistive properties of multi-walled carbon nanotube/polymer composite films aligned by an electric field, Carbon 49 (9) (2011) 2989–2997.
[65] H. Zhang, N. Liu, Y. Shi, W. Liu, Y. Yue, S. Wang, Y. Ma, L. Wen, L. Li, F. Long, Z. Zou, Y. Gao, Piezoresistive sensor with high elasticity based on 3D hybrid network of Sponge@CNTs@Ag NPs, ACS Appl. Mater. Interfaces 8 (34) (2016) 22374–22381.